Environ Fluid Mech (2009) 9:427–441
DOI 10.1007/s10652-009-9130-y

ORIGINAL ARTICLE

Energy dissipation, flow resistance and gas-liquid interfacial area in skimming flows on moderate-slope stepped spillways

Stefan Felder · Hubert Chanson

Received: 16 October 2008 / Accepted: 9 March 2009 / Published online: 22 March 2009

Abstract With the re-evaluation and revision of a number of design floods, several embankment overtopping protection systems have been developed and a common technique is the construction of a stepped spillway on the downstream slope. For such moderate slope stepped channels, detailed air–water flow measurements were performed in a large facility with a focus on the rate of energy dissipation, flow resistance, air–water interfacial areas and re-aeration rates. Past and present experimental results showed a significant aeration of the flow. The median dimensionless residual head was about $3 \times d_c$ for the 21.8° sloping chute and smaller than that for flatter slopes ($\theta = 3.4°$ and 15.9°). The flow resistance results yielded an equivalent Darcy friction factor of about 0.25 implying a larger flow resistance for the 21.8° slope angle than for smaller slope angles. The re-aeration rate was deduced from the integration of the mass transfer equation using measured air–water interfacial areas and air–water flow velocities. The results suggested an increasing re-aeration rate with increasing rate of energy dissipation. The stepped invert contributed to intense turbulence production, free-surface aeration and large interfacial areas. The experimental data showed however some distinctive seesaw pattern in the longitudinal distribution of air–water flow properties with a wave length of about two step cavities. While these may be caused by the interactions between successive adjacent step cavities and their interference with the free-surface, the existence of such "instabilities" implies that the traditional concept of normal flow might not exist in skimming flows above moderate-slope stepped spillways.

Keywords Stepped spillways · Aeration · Energy dissipation · Flow resistance · Re-oxygenation

S. Felder · H. Chanson (✉)
School of Civil Engineering, The University of Queensland, Brisbane, QLD 4072, Australia
e-mail: h.chanson@uq.edu.au
URL: http://www.uq.edu.au/~e2hchans/

Fig. 1 Stepped spillway of Salado Creek Dam Site 15R (Courtesy of Craig SAVELA, USDA-NRCS-NDCSMC)—Roller compacted concrete construction, $\theta = 21.8°$, $h = 0.61$ m

1 Introduction

In recent years, the design floods of a number of dams were re-evaluated and the revised flows were often larger than those used for the original designs. In many cases, the occurrence of these revised design floods would result in dam overtopping because of the insufficient storage and spillway capacity of the existing reservoir, with catastrophic consequences for embankment structures. A number of embankment overtopping protection systems were developed [2] and a common technique is the construction of a stepped spillway on the downstream slope (Fig. 1). Figure 1 illustrates an embankment whose primary spillway is a stepped spillway on the embankment slope. Stepped spillways are designed to increase the rate of energy dissipation on the chute [10] and it is essential therefore to predict accurately the turbulent dissipation above the steps for large discharges per unit width corresponding to the skimming flow regime. Skimming flows are highly aerated [16,30,34]. Through the air–water interface, air is continuously trapped and released, and the resulting two-phase mixture interacts with the flow turbulence yielding a complicated air–water structure. The high level of free-surface aeration is a characteristic feature of stepped chute flows, and a number of in-stream stepped cascades were built along polluted and eutrophic streams to re-oxygenate the water. For example, besides the Calumet waterway; downstream of the Petit-Saut dam [25,36]. The re-oxygenation performances of a 1.4 m high stepped cascade were recently tested by [39], and the results showed that the re-oxygenation rate may be derived from the integration of the mass transfer equation using measured air–water flow properties.

Herein two-phase turbulent flow measurements were conducted in a large facility with a channel slope angle of 21.8° (1V:2.5H). The focus of the new study is a detailed investigation of the air–water flow properties to complement similar, earlier studies (Table 1). New experiments were performed with dimensionless discharge d_c/h between 1.17 and 3.16, and Reynolds numbers ranging from $1.7\,10^5$ to $7.2\,10^5$, where d_c is the critical flow depth and h is the vertical step height. Based upon detailed air–water flow measurements, the data were analysed in terms of the rate of energy dissipation, flow resistance and air–water interfacial areas, and the results were compared with relevant literature. It is the aim of this work to characterise the energy dissipation performances, together with their aeration potential in terms of dissolved oxygen, of moderate slope stepped spillways.

2 Experimental facilities

New experiments were conducted at the University of Queensland in a 3.2 m long, 1 m wide chute (21.8°slope) with flow rates ranging from 43 to 150 L/s. The chute consisted of a

Table 1 Experimental observations of change in flow regimes on moderate slope stepped spillways

Reference	Slope θ degree	h m	d_c/h NA-TRA	d_c/h TRA-SK	Remarks
(1)	(2)	(3)	(4)	(5)	(6)
Horizontal steps					
Present study	21.8	0.05	0.6	1.0	Series BT_07 and FC_07.
[7]	21.8	0.10	0.5	0.95	Series GH_06.
[16]	21.8	0.10	0.53	0.97	Series TC_200.
[40]	18.8	0.05	0.78	1.05	
	18.8	0.025	0.78	1.05	
[21]	15.9	0.05	0.6	1.25	
	15.9	0.10	0.6	1.25	
[16]	15.9	0.10	0.75	1.2	Series TC_201.
[40]	5.7	0.05	0.76	1.25	
	5.7	0.025	0.76	1.25	
[14]	3.4	0.143	1.0	–	Series CR_98.
	3.4	0.0715	1.0	1.2	Series EV200.
Inclined downward steps					
[35]	21.8	0.04	–	2.1	Wedge-shaped blocks.
	21.8	0.016	–	2.1	

Notes d_c critical flow depth, *h* vertical step height, *NA-TRA* change from nappe to transition flow regimes, *TRA-SK* change from transition to skimming flow regimes

broad-crest followed by 20 identical steps (h = 0.05 m, l = 0.125 m) (Fig. 2). The cascade geometry and range of flow rates were selected to be a 1:2 scale model of the geometry used by [7] and [16]. The open channel facility is a permanent facility and the inflow quality has been verified in this and previous studies [23,28]. Waters are supplied by a pump controlled with adjustable frequency AC motor drive enabling an accurate discharge adjustment. The water discharge was measured from the upstream head above the crest, and the head-discharge relationship was checked with detailed velocity distribution measurements on the crest itself [23]. Clear-water flow depths were measured with a point gauge. The air–water flow properties were recorded using a single-tip resistivity probe ($\emptyset = 0.35$ mm, Pt) and a double-tip resistivity probe ($\emptyset = 0.25$ mm, Pt). In the latter, the two tips were aligned in the direction of the flow and the longitudinal separation was 7.0 mm. Both phase detection probes were excited by an electronic system (Ref. UQ82.518) designed with a response time $<10\mu$s and calibrated with a square wave generator. The probe signals were sampled at 20 kHz per sensor for 45 s. The translation of the probes in the direction normal to the pseudo-bottom formed by the step edges was controlled by a fine adjustment traverse mechanism connected to a Mitutoyo^{TM} digimatic scale unit with an accuracy of <0.2 mm.

2.1 Experimental flow conditions

On a stepped chute, the waters flow as a succession of free-falling nappes (i.e. nappe flow) at low flow rates. At large flow rates with an identical chute geometry (step height, mean

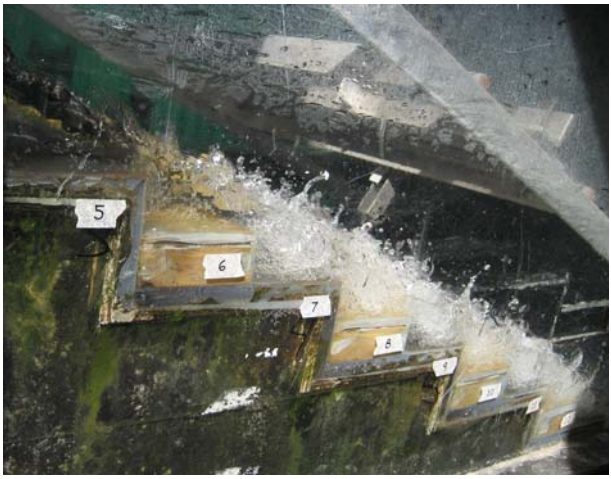

Fig. 2 Photograph of skimming flow in the stepped chute highlighting the inception point of free-surface aeration between step edges 6 and 7—Flow condition: $\theta = 21.8°$, $h = 0.05\,\text{m}$, $d_c/h = 1.17$, $Q_w = 0.0436\,\text{m}^3/\text{s}$, $\text{Re} = 1.7\,10^5$, shutter speed: 1/1,500 s

slope), the water skims over the pseudo-invert formed by the step edges (i.e. skimming flow). For some intermediate discharges, a transition flow regime is observed, characterised by a chaotic behaviour and strong splashing and droplet projections downstream of the inception point of free-surface aeration.

The present observations of changes in flow regimes are summarised in Table 1 (columns 4 and 5) together with earlier observations. Columns 4 and 5 give the characteristic dimensionless discharges d_c/h, and the present data are compared with earlier results on chute slope angles ranging from 3.4° (1V:16.8H) to 21.8° (1V:2.5H). The results and their trend were in agreement with the literature [9,10] suggesting no effect of the step height on the change in flow regimes (Fig. 3). Figure 3 presents a comparison of moderate slope data (Table 1) together with the data reported by Chanson ([10], p. 24) for steeper slopes. It shows that all data gave a consistent trend. Note that the graph does not include the data of [35] and [33] for inclined steps, nor pooled step data reported by [10].

The air–water flow measurements were conducted in the skimming flow regime with dimensionless discharge d_c/h between 1.17 and 3.16. The flow conditions corresponded to flow Reynolds numbers ranging from $1.7\,10^5$ to $7.2\,10^5$, where the Reynolds number was defined in terms of the mean flow velocity and hydraulic diameter. The probe sensors were located on the channel centreline at step edges for all flow rates. Further details on the experiments and results are reported in [19].

2.2 Data analysis

The analysis of the phase-detection probe signals provided point measurements of the void fraction C and bubble count rate F defined as the number of bubbles, or droplets, impacting a probe sensor per second. The double-tip conductivity probe measurements provided additionally the mean air–water interface velocity V, chord length distributions and air–water interface area at various positions within a cross-section.

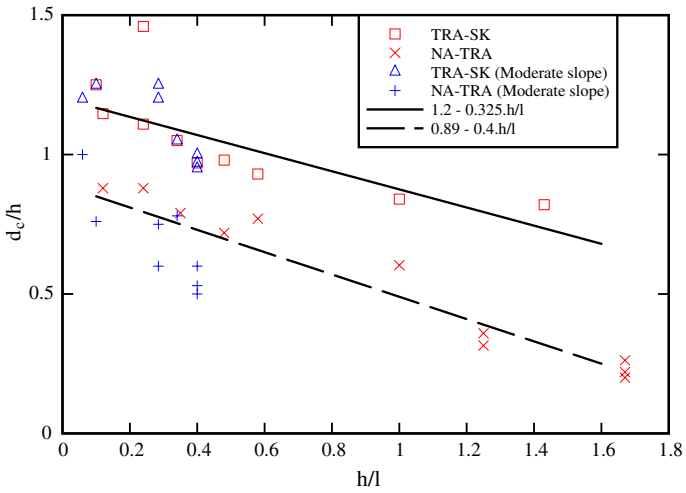

Fig. 3 Flow conditions for the change from nappe to transition flows (NA-TRA) and transition to skimming flows (TRA-SKI)—Comparison between moderate slope data (Fig. 1) [Blue symbols] and steep stepped slopes ([10], pp. 20–21) [Red symbols], and empirical correlations proposed by [10], pp. 18–19 [Black lines]

For any bubble shape, size distribution and chord length distribution, the specific air–water interface area may be estimated as:

$$a = 4\frac{F}{V} \tag{1}$$

where a is air–water interface area per unit volume. Equation 1 is valid for bubbly flows for ellopsoidal bubbles. In regions of higher air content ($C > 0.3$ to 0.4), the flow structure is more complex and Eq. 1 is simply equal to twice the number of air–water interfaces per unit length of air–water mixture ($a \propto 2\,F/V$).

2.3 Data accuracy and measurement errors

The data accuracy was typically $\Delta C/C < 2\%$ and $\Delta V/V < 5$ to 10% for void fractions between 0.03 and 0.95 and time-averaged velocities >0.5 m/s [15,38]. The smallest detectable chord length size was 0.35 mm with the single-tip probe and 0.25 mm with the double-tip probe for the observed velocities and selected sampling rate (20 kHz). The accuracy on the bubble count rate was a function of the bubble size distributions. In the present study, the characteristic bubble size was about one order of magnitude greater than the double-tip probe sensor. The accuracy on bubble count rate was about $\Delta F/F < 5\%$, yielding errors on the specific interface area <10–20%.

3 Basic observations

In transition and skimming flows, the free-surface was clear and transparent on the upper steps. Significant aeration took place when the turbulence generated by the step cavities reached the free-surface. This location is called the inception point of free-surface aeration.

	θ (deg.)	h (m)
Present study	21.8	0.05
[7]	21.8	0.10
[21]	15.9	0.05
[16]	15.9	0.10

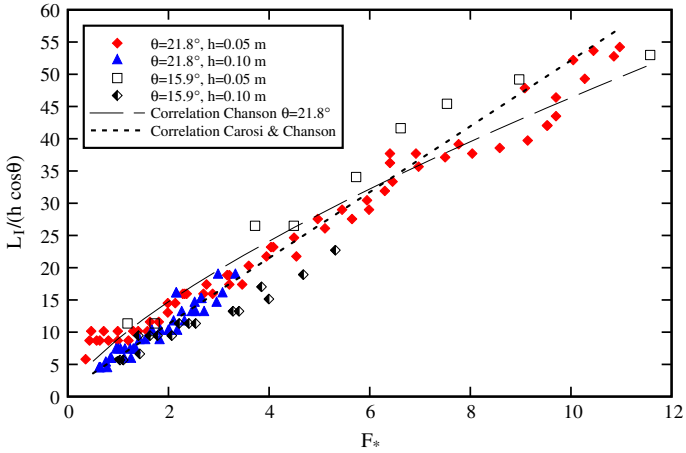

Fig. 4 Dimensionless location of the inception point of free-surface aeration on moderate slope stepped spillways—Comparison between experimental data and the correlations of [9] ($\theta = 21.8°$) and of [7]

Downstream the turbulence next to the free-surface is large enough to initiate substantial flow aeration as illustrated in Fig. 2.

The location of the inception point of free-surface aeration was recorded in transition and skimming flows. The results are plotted in Fig. 4 where the present data are reported as $L_I/(h\ \cos\theta)$ as a function of the Froude number F_*. L_I is the streamwise distance from the downstream end of the crest, $h\ \cos\theta$ is the step cavity height normal to the flow direction, and F_* is a Froude number defined in terms of the step roughness:

$$F_* = \frac{q_w}{\sqrt{g\ \sin\theta\ (h\ \cos\theta)^3}} \tag{2}$$

with q_w the water discharge per unit width, g the gravity acceleration and θ the angle between the pseudo-bottom formed by the step edges and the horizontal. In Fig. 4, the present data are compared with earlier studies on similar moderate slopes. The data are also compared with the empirical correlation:

$$\frac{L_I}{h\ \cos\theta} = 9.72\ (\sin\theta)^{0.0796}\ F_*^{0.713} \tag{3}$$

developed originally for steep stepped channels [9]. They are further compared with the simpler correlation of [7] developed for $\theta = 21.8°$:

$$\frac{L_I}{h\ \cos\theta} = 1.05\ +\ 5.11\ F_* \qquad \theta = 21.8° \text{ and } 0.45 < d_c/h < 1.6 \tag{4}$$

Figure 4 shows a close agreement between all the data suggesting that the dimensionless position of the inception point for free-surface aeration is independent of the step height and relatively little affected by the bed slope for $15.9° \leq \theta \leq 21.8°$. The data illustrate further

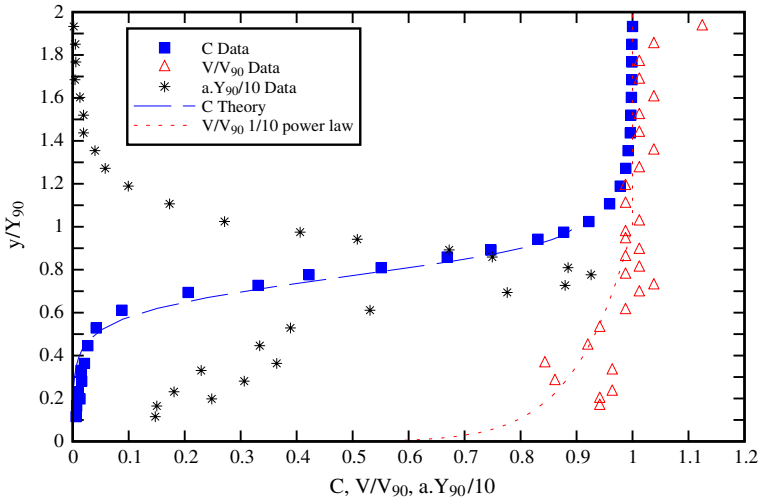

Fig. 5 Dimensionless distribution of void fraction, air–water velocity and specific interface area—$Q_w = 0.1222\,m^3/s$, $d_c/h = 2.39$, $Re = 5.1\,10^5$, Step edge 18, $Y_{90} = 0.061m$, $V_{90} = 3.46\,m/s$—Comparison with Eqs. 5 and 8

that Eq. 3 is also valid for moderate slopes. Equation 3 was successfully compared with steep slope prototype data [10] and the present results highlight its wide range of applications.

Typical dimensionless distributions of void fraction, velocity and specific interface area measured downstream of the inception point of free-surface aeration are presented in Fig. 5. The blue square are void fraction data, the empty triangles are the air–water velocity data V/V_{90} and the asterisks are specific interface area data $a\,Y_{90}/10$, where Y_{90} is the characteristic distance where $C = 0.9$, and V_{90} is the characteristic velocity where $C = 0.9$. The data presented in Fig. 5 were measured four step cavities downstream of the inception point of free-surface aeration. The void fraction data compared favourably with an advective diffusion model developed for smooth-invert chute flows:

$$C = 1 - \tanh^2\left(K' - \frac{y'}{2\,D_o} + \frac{\left(y' - \frac{1}{3}\right)^3}{3\,D_o}\right) \tag{5}$$

where $y' = y/Y_{90}$, y is the distance normal to the pseudo-bottom formed by the step edges, K' is an integration constant and D_o is a function of the depth-averaged void fraction C_{mean} only:

$$K' = 0.32745 + \frac{1}{2\,D_o} - \frac{8}{81\,D_o} \tag{6}$$

$$C_{mean} = 0.762\,(1.043 - \exp(-3.61\,D_o) \tag{7}$$

Equation 5 was developed by [13,16], and it is shown in Fig. 5.

The velocity measurements performed at step edges showed that, within the main body of the flow ($C < 90\%$), the data compared favourably with a power law:

$$\frac{V}{V_{90}} = y'^{1/N} \tag{8}$$

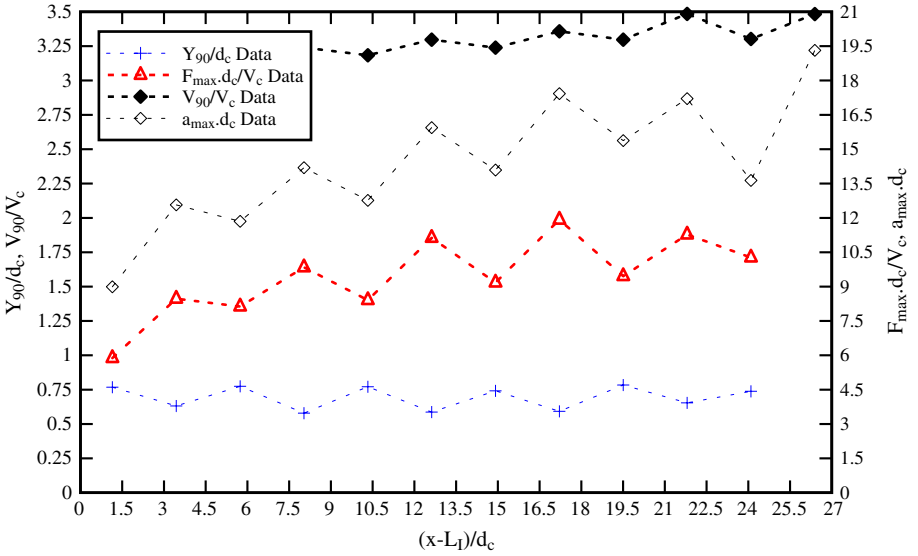

Fig. 6 Longitudinal dimensionless distributions of characteristic air–water depth Y_{90}/d_c, velocity V_{90}/V_c, maximum bubble count rate $F_{max}d_c/V_c$ and maximum specific interface area $a_{max}d_c$—Flow conditions: $Q_w = 0.044\,m^3/s$, $d_c/h = 1.17$, $Re = 1.7\,10^5$, measurements conducted at step edges

In the present study, the velocity power law exponent 1/N was 1/10 in average (i.e. $N = 10$), although it varied between adjacent step edges. Such fluctuations were believed to be caused by some interference between adjacent shear layers and cavity flows. In the upper flow region ($y > Y_{90}$), the velocity profile was pseudo-uniform:

$$\frac{V}{V_{90}} = 1 \tag{9}$$

This trend (Eq. 9) implied that the spray was little affected by air resistance. The result was consistent with the earlier findings of [7] in a stepped spillway model, and [18] and [6] who investigated high-velocity water jets discharging into air. Equations 8 and 9 are shown in Fig. 5, and the agreement with experimental data was consistent with earlier studies [7,30].

The dimensionless distributions of air-water specific interface area showed consistently a characteristic shape with a maximum value for void fractions between 0.40 and 0.6. This is seen in Fig. 5 for one flow condition. For the present flow conditions, the data showed maximum specific interface areas of up to $330\,m^{-1}$ with depth-averaged specific interface area up to $190\,m^{-1}$.

A characteristic feature of all experiments was a distinct seesaw pattern in terms of the longitudinal distributions of dimensionless air–water depth Y_{90}/d_c, dimensionless maximum bubble count rate $F_{max}d_c/V_c$ and maximum specific interface area $a_{max}d_c$, where V_c is the critical flow velocity (Fig. 6). This is illustrated in Fig. 6 for one flow rate, but the trend was similar for all investigated flow conditions. Such a seesaw pattern was previously reported, for example by [30] ($\theta = 53°$), [16] ($\theta = 22°$), and Gonzalez, and [11] ($\theta = 16°$). It is further discussed below. Also seen in Fig. 6, the maximum specific interface area and bubble count rate did not reach uniform equilibrium before the end of the chute. The dimensionless maximum bubble count rate and interface area increased sharply with longitudinal distance

immediately downstream of the inception point (i.e. $(x - L_I)/d_c < 10$), while they continued to increase gradually with increasing distance further downstream (Fig. 6).

4 Energy dissipation and flow resistance

4.1 Energy dissipation

On the stepped chute, the skimming flows dissipated a major proportion of the flow kinetic energy. The rate of energy dissipation $\Delta H/H_{max}$ and the dimensional residual energy H_{res}/d_c were estimated at three steps along the chute (steps 10, 18 and 20) based upon the air–water flow measurements. Herein H_{max} is the upstream total head above the sampling location (step 10, 18 or 20), $\Delta H = H_{max} - H_{res}$, and the residual head H_{res} is the specific energy of the flow at the sampling location:

$$H_{res} = d \cos\theta + \frac{U_w^2}{2\,g} \tag{10}$$

where U_w is the flow velocity ($U_w = q_w/d$), q_w is the water discharge per unit width and d is the equivalent clear-water depth defined as:

$$d = \int_{y=0}^{Y_{90}} (1 - C)\, dy \tag{11}$$

with y the distance normal to the pseudo-bottom formed by the step edges. The present results showed a decreasing rate of energy dissipation on the stepped chute with increasing discharge from about $\Delta H/H_{max} = 80\%$ for $d_c/h < 1.2$ to <60% for $d_c/h > 3$. The trend was consistent with earlier studies [9,30] and very close to the results of [7] with the same bed slope.

For design engineers, the dimensionless residual head H_{res}/d_c is a critical parameter since it characterises the kinetic energy to be dissipated in a downstream stilling structure. The residual energy data are shown in Fig. 7 together with earlier experimental results. The comparative data sets regroup results derived from detailed air–water flow measurements on three chute slopes ($\theta = 3.4$, 15.9° and 21.8°) and for a range of step heights ($0.05 \leq h \leq 0.143$ m), as well as clear-water flow data for one slope ($\theta = 26.6°$) and two step heights (h = 0.025 and 0.05 m). The comparison implied that the dimensionless residual head was about $2.7 \leq H_{res}/d_c \leq 3.1$ with a median value of 3.0 for $\theta = 21.8$ and 26.6°, and between $3.7 \leq H_{res}/d_c \leq 5$ with a median value of 4.5 for $\theta = 3.4$ and 15.9°, independently of the step height (Fig. 7). Note that, for the small slopes ($\theta \leq 16°$), there appeared to be some dependency of the residual energy with the dimensionless discharge d_c/h; but, for larger bed slopes, the data appeared to be independent of the flow rate.

Practically, the present results were obtained with a fully-developed, aerated flow at the chute downstream end. For larger discharges, the flow might not be fully-developed before the downstream end, and the residual energy could be considerably larger [10,24,31].

4.2 Flow resistance

On the stepped chute, the skimming flows were characterised by significant form losses. Downstream of the inception point of free-surface aeration, the average shear stress between

θ (°)	h (m)	Instrumentation	Reference
21.8	0.05 0.10	Single-tip conductivity probe (∅=0.35 mm)	Present study [7]
15.9	0.05 0.10	Single-tip conductivity probe (∅=0.35 mm) Double-tip conductivity probe (∅=0.025 mm)	[21] [16, 20]
3.4	0.07 0.143	Single-tip conductivity probe (∅=0.35 mm)	[14]
26.6	0.025 0.050	Pitot tube	[31]

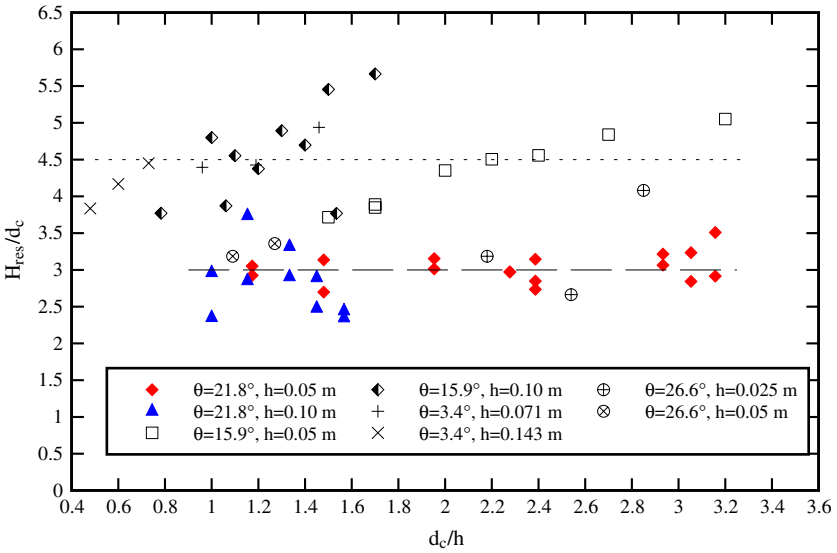

Fig. 7 Dimensionless residual energy at the downstream end of the stepped chute—Median values are shown in dotted/dashed lines—Comparison with non-aerated flow results of [31]

the skimming flow and the cavity recirculation was deduced from the measured friction slope S_f:

$$f_e = \frac{8\ \tau_o}{\rho_w\ U_w^2} = \frac{8\ g\ S_f \left(\int_{y=0}^{Y_{90}} (1 - C)\ dy \right)}{U_w^2} \tag{12}$$

where f_e is the equivalent Darcy-Weisbach friction factor, and the friction slope $S_f = -\partial H/\partial x$ is the slope of the total head line [11,27]. Equation 12 gives an estimate of the Darcy-Weisbach friction factor in the air–water flow region. The flow resistance results are presented on Fig. 8. In Fig. 8, the friction factor data are plotted as a function of the dimensionless step roughness height $h\ \cos\theta/D_H$, where D_H is the hydraulic diameter. In average, the equivalent Darcy friction factor was $\overline{f_e} \approx 0.25$ downstream of the inception point of free-surface aeration for the present study.

The present results are compared with previous studies in Fig. 8, including two sets of prototype observations (Dneiper and Brushes Clough) and several laboratory studies. All the laboratory data were close (Fig. 8) and suggested a larger flow resistance for $\theta = 21.8°$ than for the smaller slope angles. This trend was consistent with the findings of [22,26] and [32] although the discrepancy with the Brushes Clough prototype data remains unexplained [17].

θ (°)	h (m)	Comment	Reference
21.8	0.05 0.10	Laboratory model. Horizontal steps	Present study [7]
15.9	0.05 0.10	Laboratory model. Horizontal steps	[21] [16, 20]
3.4	0.07	Laboratory model. Horizontal steps	[14]
5.7, 11.3, 18.8	0.025 & 0.05	Laboratory model (Nihon University). Horizontal steps	[17, 40]
8.75	0.405	Prototype data. Dneiper hydropower plant. Wedge-shaped blocks (horizontal).	[26]
18.4	0.19	Prototype data. Brushes Clough dam spillway. Wedge-shaped block (inclined downwards).	[3]

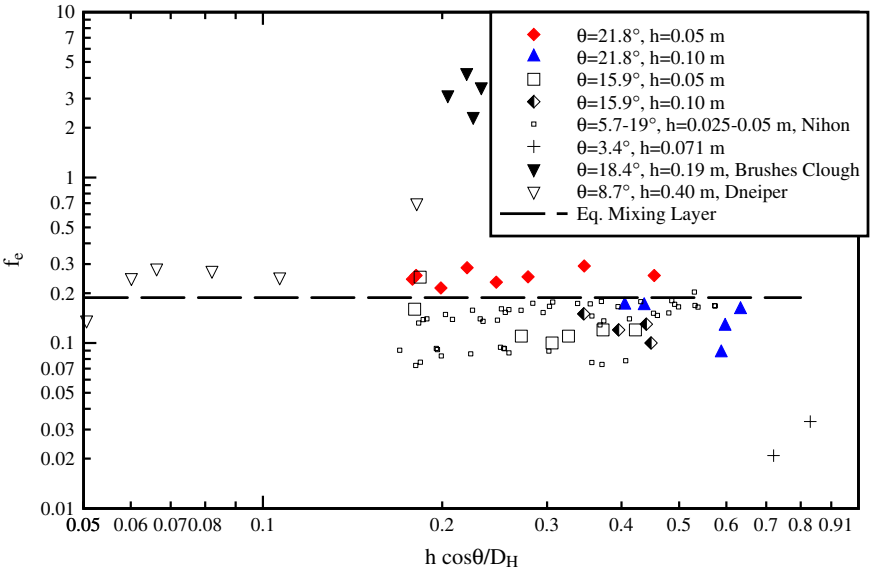

Fig. 8 Darcy–Weisbach friction factor in air–water skimming flows down moderate-slope stepped spillways

The flow resistance data were compared also with a simplified analytical model of the pseudo-boundary shear stress in the developing shear layer downstream of each step edge that may be expressed in dimensionless form as: $f = 2/(K\sqrt{\pi})$ where 1/K is the dimensionless expansion rate of the shear layer [17,21]. It predicts $f \approx 0.2$ for K = 6 that is close to the observed friction factors (Fig. 8).

Lastly, it must be noted that the results shown in Fig. 8 applied to the aerated flow region only. In the developing boundary layer region, [1] derived the flow resistance by applying an integral momentum method to PIV measurements and their results yielded f = 0.125 for $d_c/h = 2.1$ and $Re = 4.4\,10^5$.

5 Re-aeration rate

During the present study, the phase-detection probe data showed a preponderance of millimetric size bubbles, and the results gave depth-averaged mean specific area a_{mean} ranging from 30 to 190 m^{-1} that were of the same magnitude as earlier studies [15,39]. The aeration

θ (°)	h (m)	Instrumentation	Reference
21.8	0.05	Double-tip conductivity probe (∅=0.25 mm)	Present study
	0.10	Double-tip conductivity probe (∅=0.25 mm & 0.025 mm)	[7, 16]
3.4	0.143	Single-tip conductivity probe (∅=0.35 mm)	[14]
3.4	0.143	Dissolved oxygen measurements	[39]

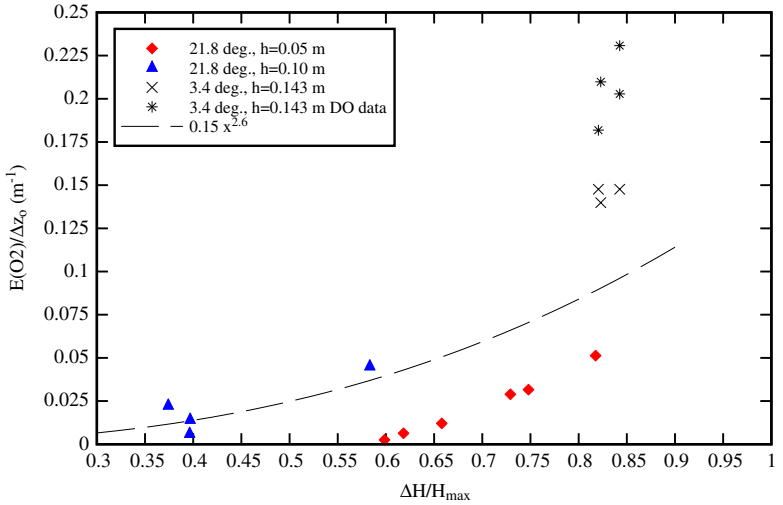

Fig. 9 Aeration efficiency per metre drop in invert elevation $E(O_2)/\Delta z_o$ in terms of dissolved oxygen at 20 Celsius at the downstream end of the stepped chute—Comparison between dissolved oxygen measurements and the integration of the mass transfer Eq. 13

efficiency of the stepped spillway system was deduced from the basic mass transfer law. For volatile chemicals (e.g. oxygen in water), the mass transfer equation at steady state yields:

$$\frac{\partial}{\partial x} C_{gas} = \frac{k_L\ a}{U_w} \left(C_{sat} - C_{gas}\right) \tag{13}$$

where C_{gas} is the concentration of the dissolved chemical in liquid, x is the longitudinal distance in the flow direction, C_{sat} is the concentration of dissolved gas in water at equilibrium and K_L is the liquid film coefficient. [29] showed that the mass transfer coefficient K_L is almost constant regardless of bubble sizes and flow situations.

Equation 13 was integrated using the measured specific interface areas and air–water flow velocities. The integration provided an estimate of the mass transfer rate. Typical results are presented in Fig. 9. Figure 9 shows the aeration efficiency per metre drop in invert elevation in terms of dissolved oxygen at 20 Celsius, standard pressure and zero salinity as a function of the measured rate of energy dissipation $\Delta H/H_{max}$. The data are compared with earlier studies, and with the dissolved oxygen measurements of [39] on a flat stepped channel ($\theta = 3.4°$, h = 0.143 m).

The results highlighted an increasing re-aeration rate of the flow with increasing rate of energy dissipation (Fig. 9). This is seen in Fig. 9. The finding was consistent with the results of [7] who linked turbulent energy dissipation with large-scale vortices and strong interactions with the free-surface aeration. Physically, the stepped invert contributed to intense turbulence production, and some turbulent energy was dissipated in the bulk of the flow through droplet ejections and air bubble entrapment. These led to an enhancement in air–water interfacial area and hence to an enhanced rate of re-aeration. Despite some scatter, the data implied

a monotonic increase in aeration performances with increasing rate of energy dissipation (Fig. 9). For the limited data set, a crude correlation is:

$$\frac{E(O_2)}{\Delta z_o} = 0.15 \left(\frac{\Delta H}{H_{max}}\right)^{2.6} \quad (14)$$

where Δz_o is the total drop in invert elevation (in m) and $E(O_2)$ is the aeration efficiency in terms of dissolved oxygen.

6 Discussion

In a skimming flow, substantial aeration and rapidly varied flow conditions take place at the inception point of free-surface aeration [8,10]. Downstream the flow is gradually-varied and fully-developed, and substantial air entrainment is observed. Further downstream, the depth-averaged void fraction C_{mean}, characteristic depth Y_{90}/d_c and velocity V_{90}/V_c seemed to reach some asymptotic values. But the results highlighted a distinctive seesaw pattern with wave length of about two step cavities (Fig. 6). It is believed that the pattern was caused by the vortex shedding in the shear layers downstream of each step edge, the interactions between successive adjacent step cavities and their interference with the free-surface [16,21,37]. A similar observation derived from the re-analysis of earlier data sets [5,30]. Interestingly the present data showed a monotonic increase in maximum bubble count rate and air–water interface area that did not reach any equilibrium before the downstream end of the chute (Fig. 6).

Altogether the data trend yield some fundamental questions: (a) how do we define uniform equilibrium flow conditions (normal flow conditions) in skimming flow above a stepped spillway ? (b) is there an unique set of normal flow conditions for a given discharge on a stepped chute ? and (c) do the flow properties alternate between several modes of excitation which may be regarded as unstable equilibrium conditions ? The concept of uniform equilibrium flow conditions (normal flow) was developed for smooth-invert chutes e.g. [4,11,27]. It is not valid for skimming flows on a stepped chute. It was recently argued that "*flow resistance in skimming flows is not an unique function of the flow rate and chute geometry*" and the form drag processes in skimming flows "*may present several modes of excitation that are function of the inflow condition, [...] cavity dimensions, cavity aeration and compliance of the stepped invert*" [12,13]. In a 24 m long chute, [14] highlighted the longitudinal variations of the air–water flow properties between step edges, although uniform equilibrium flow conditions were not achieved at the downstream end of their chute despite near full-scale prototype dimensions. Experimental evidences tended overall to refute the uniqueness of normal flow conditions in skimming flows, although further works are required to present a conclusive statement.

7 Conclusion

Detailed two-phase turbulent flow measurements were performed in a large facility with a moderate slope stepped invert (1V:2.5H). The experimental data were analysed in terms of the rate of energy dissipation, flow resistance, air–water interfacial areas and re-aeration rates, while the results were compared with relevant literature. The data demonstrated significant aeration of the flow for all investigated conditions, with depth-averaged specific interface area between 30 and 190 m^{-1}, and maximum specific interface areas of up to 330 m^{-1}. The median dimensionless residual head was about $H_{res}/d_c = 3.0$ for $\theta = 21.8°$, while the

re-analysis of earlier data sets gave $H_{res}/d_c = 4.5$ for smaller slope ($\theta = 3.4°$&$15.9°$). The results were found to be independent of step heights and discharges. The flow resistance results yielded an equivalent Darcy friction factor $\overline{f_e} \approx 0.25$ downstream of the inception point of free-surface aeration. A comparison with earlier studies showed a good agreement although it suggested a larger flow resistance for $\theta = 21.8°$ than for the smaller slope angles.

The rate of re-aeration was deduced from the integration of the mass transfer equation using measured interfacial areas. The results implied an increasing re-aeration of the flow with increasing rate of energy dissipation for the same flow rate. It is believed that the stepped invert contributed to intense turbulence production, and some turbulent energy was dissipated in the bulk of the flow through droplet ejections and air bubble entrapment enhancing the air–water interfacial area.

The experimental data showed however some distinctive seesaw pattern in the longitudinal distribution of air–water flow properties with a wave length of about two step cavities. It is thought that the trend was caused by the interactions between successive adjacent step cavities and their interference with the free-surface. The existence of such "instabilities" implies that the traditional concept of normal flow might not exist in skimming flows above moderate-slope stepped spillways.

Acknowledgments The writers thank Mr G. Illidge for his assistance. They acknowledge the helpful comments of both reviewers. The second author acknowledges the financial support of the Australian Research Council and the University of Queensland.

References

1. Amador A, Sanchez-Juny M, Dolz J (2006) Characterization of the non-aerated flow region in a stepped spillway by PIV. J Fluids Eng, ASME 128(6):1266–1273. doi:10.1115/1.2354529
2. ASCE Task Committee (1994) Alternatives for overtopping protection of dams. ASCE, New York, 139 pp (Task Committee on Overtopping Protection)
3. Baker R (1994) Brushes clough wedge block spillway—progress report no 3. SCEL project report no SJ542-4. University of Salford, UK, 47 pp
4. Bakhmeteff BA (1932) Hydraulics of open channels. 1st edn. McGraw-Hill, New York, 329 pp
5. Boes RM (2000) Zweiphasenstroömung und Energieumsetzung an Grosskaskaden (Two-Phase Flow and Energy Dissipation on Cascades), PhD thesis, VAW-ETH, Zürich, Switzerland (in German)
6. Brattberg T, Chanson H, Toombes L (1998) Experimental investigations of free-surface aeration in the developing flow of two-dimensional water jets. J Fluids Eng Trans ASME 120(4):738–744
7. Carosi G, Chanson H (2008) Turbulence characteristics in skimming flows on Stepped spillways. Can J Civ Eng 35(9):865–880. doi:10.1139/L08-030
8. Chamani MR (2000) Air inception in skimming flow regime over stepped spillways. In: Minor HE, Hager WH (eds) International workshop on hydraulics of stepped spillways. Balkema Publ, Zürich pp 61–67
9. Chanson H (1995) Hydraulic design of stepped cascades, channels, weirs and spillways. Pergamon, Oxford 292 pp
10. Chanson H (2001) The hydraulics of stepped chutes and spillways. Balkema , Lisse, The Netherlands 418 pp
11. Chanson H (2004) Environmental hydraulics of open channel flows. Elsevier Butterworth-Heinemann, Oxford 483 pp
12. Chanson H (2006) Hydraulics of skimming flows on stepped chutes: the effects of inflow conditions?. J Hydraul Res, IAHR 44(1):51–60
13. Chanson H, Toombes L (2001) Experimental investigations of air entrainment in transition and skimming flows down a stepped chute. Application to embankment overflow stepped spillways. Research report no CE158, Departmnt of Civil Engineering, The University of Queensland, Brisbane, Australia, 74 pp
14. Chanson H, Toombes L (2002a) Energy dissipation and air entrainment in a stepped storm waterway: an experimental study. J Irrigat Drain Eng, ASCE 128(5):305–315
15. Chanson H, Toombes L (2002b) Experimental study of gas-liquid interfacial properties in a stepped cascade flow. Environ Fluid Mech 2(3):241–263. doi:10.1023/A:1019884101405

16. Chanson H, Toombes L (2003) Strong interactions between free-surface aeration and turbulence in an open channel flow. Exp Therm Fluid Sci 27(5):525–535. doi:10.1016/S0894-1777(02)00266-2
17. Chanson H, Yasuda Y, Ohtsu I (2002) Flow resistance in skimming flows and its modelling. Can J Civ Eng 29(6):809–819. doi:10.1139/l02-083
18. Dodu J (1957) Etude de la Couche Limite d'Air autour d'un Jet d'Eau à Grande Vitesse (Study of the Boundary Layer around a High Velocity Water Jet). In: Proceedings of the 7th IAHR Congress, Lisbon, Portugal, paper D6 (in French)
19. Felder S, Chanson H (2008) Turbulence and turbulent length and time scales in skimming flows on a stepped spillway. Dynamic similarity, Physical modelling and scale effects, report no CH64/07. Division of Civil Engineering, The University of Queensland, Brisbane, Australia, 217 pp
20. Gonzalez CA (2005) An Experimental study of free-surface aeration on embankment stepped chutes. PhD thesis, Department of Civil Engineering, The University of Queensland, Brisbane, Australia, 240 pp
21. Gonzalez CA, Chanson H (2004) Interactions between cavity flow and main stream skimming flows: an experimental study. Can J Civ Eng 31(1):33–44. doi:10.1139/l03-066
22. Gonzalez CA, Chanson H (2006) Flow characteristics of skimming flows in stepped channels. Discussion. J Hydraul Eng, ASCE 132(5):537–539 doi:10.1061/(ASCE)0733-9429(2006)132:5(537)
23. Gonzalez CA, Chanson H (2007a) Experimental measurements of velocity and pressure distribution on a large broad-crested weir. Flow Meas Instrum 18(3–4):107–113. doi:10.1016/j.flowmeasinst.2007.05.005
24. Gonzalez CA, Chanson H (2007) Hydraulic design of stepped spillways and downstream energy dissipators for embankment dams. Dam Eng 17(4):223–244
25. Gosse P, Gregoire A (1997) Dispositif de Réoxygénation Artificielle du Sinnamary à l'Aval du Barrage de Petit-Saut (Guyane) (Artificial re-oxygenation of the sinnamary, downstream of Petit-Saut dam (French Guyana)). Hydroécol Appl 9(1–2):23–56 (in French)
26. Grinchuk AS, Pravdivets YP, Shekhtman NV (1977) Test of earth slope revetments permitting flow of water at large specific discharges (Gidrotekhnicheskoe Stroitel'stvo (4):22–26 (in Russian)). (Translated in Hydrotechnical Construction, 1978, Plenum Publ, pp 367–373)
27. Henderson FM (1966) Open Channel Flow. MacMillan Company, New York
28. Jempson MA (2001) Flood and debris loads on bridges. PhD thesis, University of Queensland, Department of Civil Engineering, Australia, 429 pp
29. Kawase Y, Moo-Young M (1992) Correlations for liquid-phase mass transfer coefficients in bubble column reactors with Newtonian and non-Newtonian fluids. Can J Chem Eng 70(Feb):48–54
30. Matos J (2000) Hydraulic design of stepped spillways over RCC dams. In: Minor HE, Hager WH (eds) Intl Workshop on Hydraulics of Stepped Spillways. Balkema Publ, Zürich pp 187–194
31. Meireles I, Cabrita J, Matos J (2006) Non-aerated skimming flow properties on stepped chutes over small embankment dams. In: Matos J, Chanson H (eds) Proceedings of the international junior researcher and engineer workshop on hydraulic structures, IAHR, Montemor-o-Novo, Portugal, 2–4 Sept, hydraulic model report no CH61/06, Division of Civil Engineering, The University of Queensland, Brisbane, Australia, pp 91–99
32. Ohtsu I, Yasuda Y, Takahashi M (2004) Flow Characteristics of skimming flows in stepped channels. J Hydraul Eng, ASCE, 130(9):860–869. Discussion 132(5):527–542
33. Peyras L, Royet P, Degoutte G (1991) Ecoulement et Dissipation sur les Déversoirs en Gradins de Gabions (Flows and Dissipation of Energy on Gabion Weirs). J La Houille Blanche (1):37–47 (in French)
34. Rajaratnam N (1990) Skimming Flow in Stepped Spillways. J Hydraul Eng, ASCE 116(4):587–591. Discussion 118(1):111–114
35. Relvas AT, Pinheiro AN (2008) Inception point and air concentration in flows on stepped chutes lined with wedge-shaped concrete blocks. J Hydraul Eng, ASCE 134(8):1042–1051
36. Robison R (1994) Chicago's waterfalls. Civ Eng, ASCE 64(7):36–39
37. Thorwarth J, Köngeter J (2006) Physical model tests on a stepped chute with pooled steps. Investigations of flow resistance and flow Instabilities. In: Marcano A, Martinez A (eds) Proceedings of the International symposium on hydraulic structures. IAHR, Ciudad Guayana, Venezuela, pp 477–486
38. Toombes L (2002) Experimental study of air–water flow properties on low-gradient stepped cascades. PhD thesis, Department of Civil Engineering, The University of Queensland, Brisbane, Australia
39. Toombes L, Chanson H (2005) Air–water mass transfer on a stepped waterway. J Environ Eng, ASCE 131(10):1377–1386
40. Yasuda Y, Ohtsu IO (1999) Flow Resistance of skimming flow in stepped channels. In: Proceedings of the 28th IAHR Congress. Graz, Austria, Session B14, 6 pp